Design and Experimental Implementation of a Compliant Hybrid Zero Dynamics Controller for Walking on MABEL

Koushil Sreenath, Hae-Won Park, Ioannis Poulakakis, J. W. Grizzle

***Abstract*— This paper extends the method of virtual constraints and hybrid zero dynamics, developed for rigid robots with a single degree of underactuation, to MABEL, a planar biped with a novel compliant transmission. A time-invariant feedback controller is designed for realizing exponentially stable waking gaits in such a way that the closed-loop system preserves the natural compliance of the system, and therefore the energetic benefits of springs. This is accomplished by incorporating the compliance into the hybrid zero dynamics. The compliant-hybrid-zero-dynamics-based controller is implemented experimentally and shown to realize stable walking gaits which make use of the compliance to store and return energy to the gait.**

I. Introduction

MABEL is a bipedal robot with a series-compliant actuator. It was conceived as a testbed for exploring control strategies that can take advantage of the compliance present in a system in order to achieve energy efficient, stable locomotion. Here we show how the method of virtual constraints can be used to accomplish this feedback objective.

The robot MABEL is planar, with a torso, two legs, four actuators, and a novel drivetrain that uses a set of cable-driven differentials to create a virtual prismatic leg between the hip and the toe. The differentials also introduce a compliant element, in series with an actuator along the virtual leg, such that the leg length is directly controlled by the actuator and the spring compression. Another actuator controls the angle of the virtual leg with respect to the torso. This design facilitates the placement of all actuators inside the torso and thus keeps the legs relatively light for rapid leg motion. Figure 1 illustrates the testbed. A more detailed description of the robot is presented in [2], [3], and the identification of the robot's dynamic model is reported in [4].

Compliance in legged robots is important for energy efficiency and for robust locomotion over rough terrain. Springs can be used to store and release energy to perform the negative work of redirecting the center of mass upward after leg impact [5]; they can also be used to isolate actuators from mechanical shocks arising from leg impacts with the ground. In MABEL, compliance is present in the form of a unilateral spring that compresses, but does not extend beyond its rest length. This ensures that the compliance is present when it is useful for shock attenuation and energy storage, and absent when it would be a hindrance for lifting a leg from the ground.

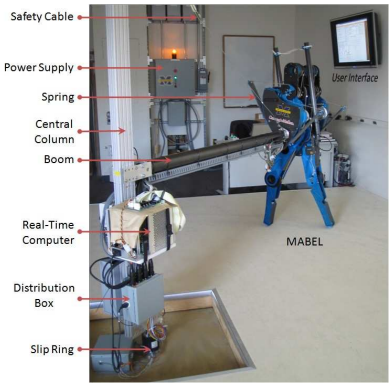

(a) (b)

Fig. 1. (a) MABEL, an experimental testbed for bipedal locomotion. The robot is planar, with a boom providing stabilization in the frontal plane. The robot's drivetrain contains springs for enchanced power efficiency. (b) The *virtual compliant leg* created by the drivetrain through a set of differentials. The coordinate system used for the linkage is also indicated. Angles are positive in the counter clockwise direction.

The presence of compliance has led to new control challenges that cannot be met with the initial theory developed for RABBIT [6]. Firstly, compliance increases the degree of underactuation, which in turn makes it more difficult to meet the invariance condition required for a hybrid zero dynamics to exist. This technical difficulty was overcome in [7] with a technique called a "deadbeat hybrid extension". A second challenge arising from compliance is how to use it effectively. A first attempt in [8] at designing a controller for a biped with springs took advantage of the compliance along a steady state walking gait, but "fought it" during transients; see [9, p. 1790]. This drawback was overcome on a hopper model in [9], [10], [11] by ensuring that the feedback action resulted in the hybrid zero dynamics (HZD) itself being compliant. The key idea was that the selection of the virtual constraints specifies the subset of the robot's generalized coordinates that are to be actively controlled. If the constraints have vector relative degree two in the sense of [12], a complement of this subset forms the zero dynamics of the closed-loop system, and hence these coordinates will remain "passive". By deliberately placing the compliance in the zero dynamics, the closed-loop system preserves the natural compliance of the system, and therefore the energetic

Koushil Sreenath and J. W. Grizzle are with the Control Systems Laboratory, Electrical Engineering and Computer Science Department, University of Michigan, Ann Arbor, MI 48109-2122, USA. {koushils, grizzle}@umich.edu

Hae-Won. Park is with the Mechanical Engineering Department, University of Michigan, Ann Arbor, MI 48109-2125, USA. parkhw@umich.edu

Ioannis Poulakakis is with the Mechanical Engineering Department, University of Delaware, Newark, DE 19716, USA. poulakas@udel.edu

This work is supported by NSF grants ECS-909300, ECS-0600869. An extended version of this paper with several other experiments and results has been submitted [1].

benefits of springs.

Motivated by these results, we extend the above work to design a compliant HZD controller for walking gaits of MABEL. The controller is implemented in real-time and experimentally validated on the robot. All prior experimental implementations of the virtual constraints have relied on local PD controllers [6], [2]. However, on MABEL, enforcing virtual constraints through PD controllers led to large tracking errors due in part to low gear ratios between the links and the actuators. These errors are very pronounced for fast walking gaits where the stance time is on the order of 300 ms. In light of this, we explore implementations of the theoretical HZD-based controller. While zero dynamics controllers are recognized to provide perfect tracking accuracy in theory, they are often criticized for being overly dependent on high model accuracy, and for being too complex to implement in real-time. Here we demonstrate, for the first time, an experimental implementation of a compliant HZD controller. The tracking accuracy attained is far better than the simple PD controllers used previously [1].

The remainder of the paper is organized as follows. Section II presents the mathematical hybrid model used for walking. Section III provides the systematic procedure based on virtual constraints that can be used to design a suite of walking gaits. Section IV presents the design of the compliant HZD controller and studies the stability of the fixed point under the action of the proposed controller. Section V presents the results of experimentally implementing the designed controller. Finally, Section VI provides concluding remarks.

II. MABEL Model

This section develops the hybrid model appropriate for a walking gait comprised of a continuous single support phase and an instantaneous double support phase. Standard hypotheses such as no slip during single support or at impact are assumed; see [13, pp. 50-51] for a complete list of assumptions. The impact model at double support is based on [14]. The single support model is a pinned, rigid, planar, 5-link kinematic chain with revolute joints [13]. Because the compliance is unilateral, it will be more convenient to model it as an external force when computing the Lagrangian, instead of including it as part of the potential energy.

A. MABEL's unconstrained Dynamics

The configuration space Q_{e} of the unconstrained dynamics of MABEL is an open simply-connected subset of $\mathbb{S}^7 \times \mathbb{R}^2$: five DOF are associated with the links in the robot's body, two DOF are associated with the springs in series with the two leg-shape motors, and two DOF are associated with the horizontal and vertical position of the robot in the sagittal plane. A set of coordinates suitable for parametrization of the robot's linkage and transmission is, $q_{\mathrm{e}} := (\ q_{\mathrm{LA_{st}}};\ q_{\mathrm{mLS_{st}}};\ q_{\mathrm{Bsp_{st}}};\ q_{\mathrm{LA_{sw}}};\ q_{\mathrm{mLS_{sw}}};\ q_{\mathrm{Bsp_{sw}}};\ q_{\mathrm{Tor}};\ p^h_{\mathrm{hip}};\ p^v_{\mathrm{hip}}\ )$, where, as in Figure 1 and [2, Fig. 3], q_{Tor} is the torso angle, and $q_{\mathrm{LA_{st}}}$, $q_{\mathrm{mLS_{st}}}$, and $q_{\mathrm{Bsp_{st}}}$ are the leg angle, leg-shape motor position and $\mathrm{B_{spring}}$ position respectively for the stance leg. The swing leg variables, $q_{\mathrm{LA_{sw}}}$, $q_{\mathrm{mLS_{sw}}}$ and $q_{\mathrm{Bsp_{sw}}}$ are defined similarly. For each leg, q_{LS} is uniquely determined from q_{mLS} and q_{Bsp} by

$$q_{LS} = 0.0318 q_{\mathrm{mLS}} + 0.193 q_{\mathrm{Bsp}}. \tag{1}$$

This reflects on the fact that the cable differentials place the spring in series with the motor, with the pulleys introducing a gear ratio. The coordinates $p^h_{\mathrm{hip}}, p^v_{\mathrm{hip}}$ are the horizontal and vertical positions of the hip in the sagittal plane. The hip position is chosen as an independent coordinate instead of the center of mass because it was observed that this choice significantly reduces the number of terms in the symbolic expression for the dynamics.

The equations of motion are obtained using the method of Lagrange. In computing the Lagrangian, the total kinetic energy is taken to be the sum of the kinetic energies of the transmission, the rigid linkage, and the boom. The potential energy is computed in a similar manner with the difference being that the transmission contributes to the potential energy of the system only through its non-elastic energy (the mass). This distinction is made since the unilateral spring is considered as an external input to the system. The resulting model of the robot's unconstrained dynamics is determined as

$$D_{\mathrm{e}}(q_{\mathrm{e}})\,\ddot{q}_{\mathrm{e}} + C_{\mathrm{e}}(q_{\mathrm{e}}, \dot{q}_{\mathrm{e}})\,\dot{q}_{\mathrm{e}} + G_{\mathrm{e}}(q_{\mathrm{e}}) = \Gamma_{\mathrm{e}}, \tag{2}$$

where, D_{e} is the inertia matrix, C_{e} contains Coriolis and centrifugal terms, G_{e} is the gravity vector, and Γ_{e} is the vector of generalized forces acting on the robot, expressed as,

$$\begin{aligned}\Gamma_{\mathrm{e}} = {} & B_{\mathrm{e}} u + E_{\mathrm{ext}}(q_{\mathrm{e}})\,F_{\mathrm{ext}} + \\ & B_{fric}\tau_{fric}(q_{\mathrm{e}}, \dot{q}_{\mathrm{e}}) + B_{sp}\tau_{sp}(q_{\mathrm{e}}, \dot{q}_{\mathrm{e}}),\end{aligned} \tag{3}$$

where the matrices B_{e}, E_{ext}, B_{fric}, and B_{sp} are derived from the principle of virtual work and define how the actuator torques u, the external forces F_{ext} at the leg, the joint friction forces τ_{fric}, and the spring torques τ_{sp} enter the model respectively. The dimension of u is four, corresponding to the two actuators on each leg for actuating leg shape and leg angle.

B. Dynamics of Stance

For modeling the stance phase, the stance toe is assumed to act as a passive pivot joint (no slip, no rebound and no actuation). Hence, the Cartesian position of the hip, $\left(p^h_{\mathrm{hip}}, p^v_{\mathrm{hip}}\right)$, is defined by the coordinates of the stance leg and torso. The springs in the transmission are appropriately chosen to support the entire weight of the robot, and hence are stiff. Consequently, it is assumed that the spring on the swing leg does not deflect, that is, $q_{\mathrm{Bsp_{sw}}} \equiv 0$. The stance configuration space, Q_{s}, is therefore a co-dimension three submanifold of Q_{e}. It follows from (1) that $q_{\mathrm{mLS_{sw}}}$ and $q_{\mathrm{LS_{sw}}}$ are related by a gear ratio; $q_{\mathrm{mLS_{sw}}}$ is taken as the independent variable. With these assumptions, the generalized configuration variables in stance are taken as $q_{\mathrm{s}} := \left(q_{\mathrm{LA_{st}}}; q_{\mathrm{mLS_{st}}}; q_{\mathrm{Bsp_{st}}}; q_{\mathrm{LA_{sw}}}; q_{\mathrm{mLS_{sw}}}; q_{\mathrm{Tor}}\right)$. Defining

the state vector $x_{\mathrm{s}} := (q_{\mathrm{s}}; \dot{q}_{\mathrm{s}}) \in TQ_{\mathrm{s}}$, the stance dynamics can be expressed in the standard form as,

$$\dot{x}_{\mathrm{s}} = f_{\mathrm{s}}(x_{\mathrm{s}}) + g_{\mathrm{s}}(x_{\mathrm{s}})u. \tag{4}$$

C. Stance to Stance Transition Map

An impact occurs when the swing leg touches the ground, modeled here as an inelastic contact between two rigid bodies. It is assumed that there is no rebound or slip at impact. Mathematically, the transition occurs when the solution of (4) intersects the co-dimension one switching manifold

$$\mathcal{S}_{\mathrm{s}\to\mathrm{s}} := \left\{ x_{\mathrm{s}} \in TQ_{\mathrm{s}} \mid p^{v}_{\mathrm{toe}_{\mathrm{sw}}} = 0 \right\}. \tag{5}$$

In addition to modeling the impact of the leg with the ground and the associated discontinuity in the generalized velocities of the robot [14], the transition map accounts for the assumption that the spring on the swing leg is at its rest length, and for the relabeling of robot's coordinates so that only one stance model is necessary. In particular, the transition map consists of three subphases executed in the following order: (a) standard rigid impact model [14]; (b) adjustment of spring rest length in the new swing leg; and (c) coordinate relabeling.

The stance to stance transition map, $\Delta_{\mathrm{s}\to\mathrm{s}} : \mathcal{S}_{\mathrm{s}\to\mathrm{s}} \to TQ_{\mathrm{s}}$, is similar to the one developed in [11, Chap. 5], [1] and further details are omitted for the sake of brevity.

D. Hybrid model of Walking

The hybrid model of walking is based on the dynamics developed in Section II-B, and transition map derived in Section II-C. The continuous dynamics with discrete state transitions is represented as,

$$\Sigma_{\mathrm{s}} : \begin{cases} \dot{x}_{\mathrm{s}} = f_{\mathrm{s}}(x_{\mathrm{s}}) + g_{\mathrm{s}}(x_{\mathrm{s}})u & x^{-}_{\mathrm{s}} \notin S_{\mathrm{s}\to\mathrm{s}} \\ x^{+}_{\mathrm{s}} = \Delta_{\mathrm{s}\to\mathrm{s}}(x^{-}_{\mathrm{s}}) & x^{-}_{\mathrm{s}} \in S_{\mathrm{s}\to\mathrm{s}} \end{cases}. \tag{6}$$

III. Gait Design using Zero Dynamics

This section presents a feedback controller for achieving exponentially stable, periodic walking gaits on MABEL. In addition to orbital stability, a key objective is to take advantage[1] of the spring in the robot's drivetrain that is placed in series with the leg-shape motor and q_{LS}. Inspired by analysis in [9, p. 1784] and [11, Chap. 6] for monopedal hoppers with compliance, this will be accomplished by controlling variables on the motor end of the spring and letting the joint end of the spring, which sees the large ground reaction forces, remain passive. In this way, the robot in closed-loop with the controller will respond to impulsive forces at impact in a manner similar to a pogo stick. In particular, the closed-loop system will use the compliance to do negative work at impact (i.e., decelerating the center of mass and redirecting it upward), instead of it being done by the actuators, thereby improving the energy efficiency of walking.

It will be shown that the method of virtual constraints and hybrid zero dynamics is flexible enough to accomplish the control objectives outlined above. The method of Poincaré is used to verify stability of the closed-loop system. Prior to experimentally testing the controller, simulations with various model perturbations are performed to establish robustness of the designed controller. The controller is then experimentally validated on MABEL.

[1]The reader wishing to understand immediately the utility of the compliance should consult Figure 10.

A. Virtual Constraint Design for Stance

Recall that virtual constraints are holonomic constraints on the robot's configuration variables that are asymptotically imposed through feedback control. They are used to synchronize the evolution of the robot's links throughout a stride in order to synthesize a gait [13]. One virtual constraint is designed per independent actuator.

The virtual constraints are parametrized by θ_{s}, a strictly monotonic function of the joint configuration variables, and can be expressed in the form

$$y = h_{\mathrm{s}}(q_{\mathrm{s}}) = H^{\mathrm{s}}_0 q_{\mathrm{s}} - h^{\mathrm{s}}_d(\theta_{\mathrm{s}}). \tag{7}$$

If a feedback can be found such that y is driven asymptotically to zero, then $H^{\mathrm{s}}_0 q_{\mathrm{s}} \to h^{\mathrm{s}}_d(\theta_{\mathrm{s}})$ and thus the controlled variables $H^{\mathrm{s}}_0 q_{\mathrm{s}}$ evolve according to the constraint $H^{\mathrm{s}}_0 q_{\mathrm{s}} = h^{\mathrm{s}}_d(\theta_{\mathrm{s}})$. Here, the controlled variables are selected to be the rotor angle of the stance leg-shape motor, $q_{\mathrm{mLS}_{\mathrm{st}}}$, the swing leg variables, $q_{\mathrm{LA}_{\mathrm{sw}}}, q_{\mathrm{mLS}_{\mathrm{sw}}}$, and the absolute torso angle q_{Tor}. Each of these variables has relative degree two. From hereon, the rotor angle of the stance leg-shape motor is simply referred to as stance motor leg shape.

1) Deciding what to control: The torso is selected as a controlled variable instead of the stance leg angle, because, for MABEL, the torso represents over 65% of the mass of the robot, and hence the position of the torso heavily influences the gait. The stance motor leg shape, $q_{\mathrm{mLS}_{\mathrm{st}}}$, is chosen instead of the stance leg shape, $q_{\mathrm{LS}_{\mathrm{st}}}$, so that the joint side of the spring remains passive, as discussed above. Mathematically, with this choice, the spring variable will become a part of the zero dynamics, thereby rendering the zero dynamics compliant. From (1), if $q_{\mathrm{mLS}_{\mathrm{st}}}$ is held constant, then $q_{\mathrm{LS}_{\mathrm{st}}}$ responds to the spring torque through $q_{\mathrm{Bsp}_{\mathrm{st}}}$. On the other hand, if $q_{\mathrm{LS}_{\mathrm{st}}}$ were selected as a controlled variable, then the actuator is forced to cancel the spring dynamics.

The swing leg virtual constraints are similar to the controlled variables on RABBIT, a robot without compliance. This is because under the assumption that the swing spring is at its rest position throughout stance, $q_{\mathrm{Bsp}_{\mathrm{sw}}} \equiv 0$, which from (1) shows that the motor leg shape, $q_{\mathrm{mLS}_{\mathrm{sw}}}$, is related to the leg shape, $q_{\mathrm{LS}_{\mathrm{sw}}}$, through a gear ratio.

In summary, the controlled variables are

$$H^{\mathrm{s}}_0 q_{\mathrm{s}} = \begin{bmatrix} q_{\mathrm{mLS}_{\mathrm{st}}} \\ q_{\mathrm{LA}_{\mathrm{sw}}} \\ q_{\mathrm{mLS}_{\mathrm{sw}}} \\ q_{\mathrm{Tor}} \end{bmatrix}, \tag{8}$$

and h^{s}_d represents the desired evolution of each of the virtual constraints, $h^{d}_{\mathrm{mLS}_{\mathrm{st}}}$, $h^{d}_{\mathrm{LA}_{\mathrm{sw}}}$, $h^{d}_{\mathrm{mLS}_{\mathrm{sw}}}$, and h^{d}_{Tor} respectively.

For MABEL, we choose θ_{s} to be the absolute angle formed by the virtual compliant leg relative to the ground, i.e.,

$$\theta_{\mathrm{s}}\left(q_{\mathrm{s}}\right) = \pi - q_{\mathrm{LA_{st}}} - q_{\mathrm{Tor}}. \tag{9}$$

2) Specification of the constraints: Virtual constraints for the stance phase of MABEL are inspired by the constraints designed for Thumper in [10], [11]. The stance phase is broken up into subphases: the motor-compression phase (*mc*), the stance-compression phase (*sc*), the stance-injection phase (*si*), and the stance-decompression phase (*sd*). The breakup into subphases facilitates the design of virtual constraints that make use of the compliance effectively. A key idea is to hold the stance motor leg shape at a constant value shortly after impact in order to allow the spring (which is in series with this actuator) to absorb the impact shock entirely. Note that if the motor position is held constant, then its velocity is zero and the motor performs no mechanical work. The spring then does the negative work of decelerating the center of mass and redirecting it upwards; the spring stores this energy and returns it later to the gait instead of the actuator doing negative work and dissipating it as heat. This effectively preserves the natural compliant dynamics of the system and prevents the actuator from fighting the spring.

Figure 2 illustrates the evolution of each of these constraints on $q_{\mathrm{mLS_{st}}}$, $q_{\mathrm{LA_{sw}}}$, $q_{\mathrm{mLS_{sw}}}$, and q_{Tor}.

Another key subphase involves the torso. Because it is heavy, we have observed that making the pre-impact torso velocity close to zero at the end of the gait helps in avoiding excessive forward pitching of the torso just after swing leg impact. This is achieved by designing the torso virtual constraint such that for the last part of the gait, the torso position is held constant, making its velocity zero.

Thus for the constraint on $q_{\mathrm{mLS_{st}}}$, the *mc* phase serves as a transient to smoothly drive the motor velocity to zero, and the *sc* phase serves to hold the motor position constant for the benefits discussed above. During the *si* phase, the motor is repositioned, which under nominal conditions, serves to straighten the stance leg during mid-stance for ground clearance. Under large perturbations, this motion will cause the actuator to inject (or remove) energy through compression (or decompression) of the spring by rapidly repositioning the motor end of the compliance. For the torso constraint, the first three phases are treated as one, which serves as a transient phase to drive the torso velocity to zero. During the *sd* phase, the torso position is held constant as discussed above. The swing leg virtual constraints are standard, and not discussed further.

***Remark** 1:* The choice of the variables to be controlled in the virtual constraints makes the zero dynamics compliant. The choice of the evolution of the virtual constraints facilitates efficient use of the compliance.

3) Discussion: The use of subphases in the evolution of the stance motor leg shape and torso introduces more independent parameters to be specified in the constraint design. One benefit is that it approximately decouples the evolution of these angles from one phase to another; changing the evolution in one phase does not strongly affect the other as long as the boundary condition is maintained. This facilitates intuitively specifying the initial shape of the virtual constraints and makes the optimization task easier. We impose $\mathcal{C}^1$ continuity between successive subphases. This ensures continuity of position and velocity at the boundary of two phases of a virtual constraint. However, acceleration, and consequently, the actuator torques, are allowed to be discontinuous at phase boundaries.

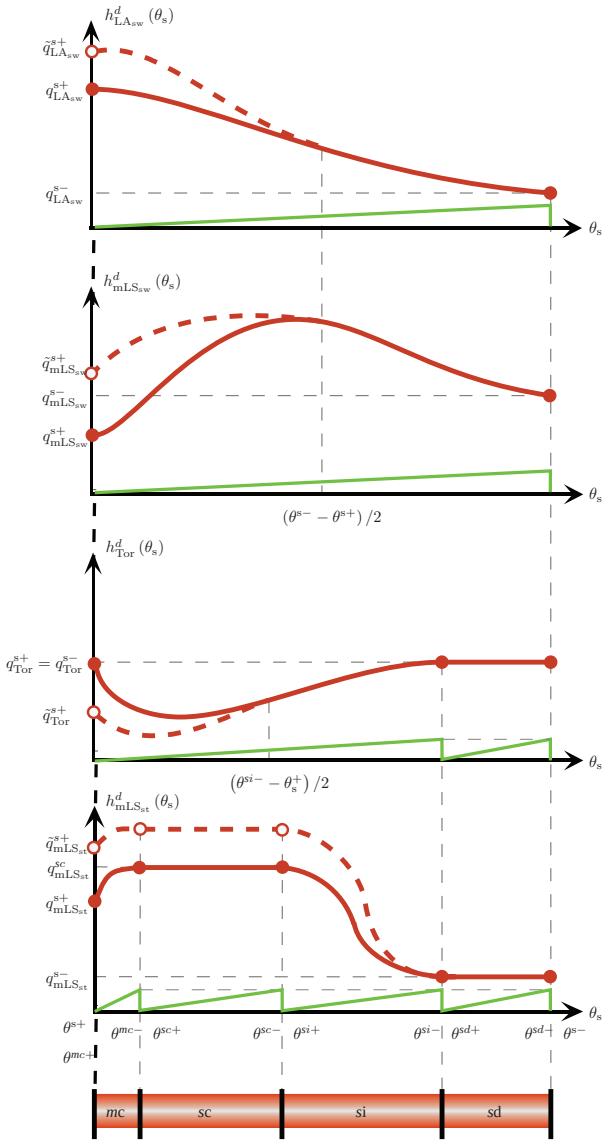

Fig. 2. The general shape of the stance phase virtual constraints. The thick (red) solid lines illustrate the evolution of each of the virtual constraints as a function of θ_{s}. Each virtual constraint is broken into subphases (*mc*, *sc*, *si*, sd), locally expressed by 5^{th} order Bézier polynomials. The thin green lines show the evolution of corresponding local s that parametrizes the local Bézier curve. The torso and swing virtual constraints combine multiple subphases. The (red) dashed lines are correction polynomials introduced to create hybrid invariance of the zero dynamics.

For later use, we can organize the virtual constraints for each phase separately. Construct the index set for the virtual constraints, $\mathcal{V} := \{\mathrm{mLS_{st}}, \mathrm{LA_{sw}}, \mathrm{mLS_{sw}}, \mathrm{Tor}\}$, and for each

$p \in \mathcal{P} := \{mc, sc, si, sd\}$, we can define the output,

$$y_p = h_p(q_s, \alpha_p) = H_0^p(q_s) - h_d^p(\theta_s, \alpha_p), \tag{10}$$

and,

$$h_d^p(\theta_s, \alpha_p) = \begin{bmatrix} h_{\mathrm{mLS_{st}}}^{d,p}(\theta_s) \\ h_{\mathrm{LA_{sw}}}^{d,p}(\theta_s) \\ h_{\mathrm{mLS_{sw}}}^{d,p}(\theta_s) \\ h_{\mathrm{Tor}}^{d,p}(\theta_s) \end{bmatrix}. \tag{11}$$

The Bézier coefficients for each phase can be organized as,

$$\alpha_p = \begin{bmatrix} \alpha_{\mathrm{mLS_{st}}}^p \\ \alpha_{\mathrm{LA_{sw}}}^p \\ \alpha_{\mathrm{mLS_{sw}}}^p \\ \alpha_{\mathrm{Tor}}^p \end{bmatrix}. \tag{12}$$

B. Stance Zero Dynamics

The organization of the stance phase into four subphases creates four continuous dynamics and discrete transitions between them. As discussed in Section III-A.3, for each phase $p \in \mathcal{P}$, an output function y_p has been associated with the continuous stance dynamics defined in (4). Differentiating the output twice[2] with respect to time results in

$$\frac{d^2 y_p}{dt^2} = L_{f_s}^2 h_p(x_s, \alpha_p) + L_{g_s} L_{f_s} h_p(q_s, \alpha_p), \tag{13}$$

where $L_{g_s} L_{f_s} h_p(q_s, \alpha_p)$ is the decoupling matrix. Under the conditions of [13, Lemma 5.1],

$$\begin{aligned} u^*(x_s, \alpha_p) := &-\left(L_{g_s} L_{f_s} h_p(q_s, \alpha_p)\right)^{-1} \\ &L_{f_s}^2 h_p(x_s, \alpha_p), \end{aligned} \tag{14}$$

is the unique control input that renders the smooth four-dimensional embedded submanifold

$$\begin{aligned} \mathcal{Z}_{\alpha_p} = \{x_s \in TQ_s \mid\ & h_p(q_s, \alpha_p) = 0, \\ & L_{f_s} h_p(x_s, \alpha_p) = 0\} \end{aligned} \tag{15}$$

invariant under the stance dynamics (4); that is, for every $z \in \mathcal{Z}_{\alpha_p}$,

$$f_p^*(z) := f_s(z) + g_s(z)\, u^* \in T_z \mathcal{Z}_{\alpha_p}. \tag{16}$$

Achieving the virtual constraints by zeroing the corresponding outputs reduces the dimension of the system by restricting its dynamics to the submanifold $\mathcal{Z}_{\alpha_p}$ embedded in the continuous-time state space TQ_s. $\mathcal{Z}_{\alpha_p}$ is called the zero dynamics manifold and the restriction dynamics $\dot{z} = f_p^*|_{\mathcal{Z}_{\alpha_p}}(z)$ is called the zero dynamics.

From Lagrangian dynamics (the derivation is standard [13, Chap. 5] and skipped for sake of brevity), a valid set coordinates on $\mathcal{Z}_{\alpha_p}$ is

$$x_{zd}^p = \begin{bmatrix} \xi_1 \\ \xi_2 \\ \xi_3 \\ \xi_4 \end{bmatrix} = \begin{bmatrix} \theta_s \\ q_{\mathrm{Bsp_{st}}} \\ \frac{\partial \mathcal{L}_s}{\partial \dot{q}_{\mathrm{Bsp_{st}}}} \\ \frac{\partial \mathcal{L}_s}{\partial \dot{q}_{\mathrm{Tor}}} \end{bmatrix}. \tag{17}$$

[2]It is straightforward to check that the variables to be controlled have vector relative degree two.

This set of coordinates explicitly contains the $\mathrm{B_{spring}}$ variable, which illustrates clearly that the zero dynamics is compliant:

$$\dot{x}_{zd}^p = \begin{bmatrix} \dot{\xi}_1 \\ \dot{\xi}_2 \\ \dot{\xi}_3 \\ \dot{\xi}_4 \end{bmatrix} = \begin{bmatrix} L_{f_s} \theta_s \\ L_{f_s} q_{\mathrm{Bsp_{st}}} \\ \frac{\partial \mathcal{L}_s}{\partial q_{\mathrm{Bsp_{st}}}} + \tau_{sp} \\ \frac{\partial \mathcal{L}_s}{\partial q_{\mathrm{Tor}}} \end{bmatrix}. \tag{18}$$

C. Event Transitions

The division of the stance phase into subphases when specifying the virtual constraints in Section III-A necessitates the specification of the transition maps between the subphases. In preparation for the next section, we model the hybrid dynamics on the zero dynamics manifold by concatenating the solutions of the parameter-dependent hybrid systems for each subphase

$$\Sigma_p : \begin{cases} x_p \in \mathcal{Z}_{\alpha_p} \\ \dot{x}_p = f_p^*(x_p) \\ \mathcal{S}_{p \to q} = \left\{x_p \in \mathcal{Z}_{\alpha_p} \mid H_{p \to q}(x_p) = 0\right\} \\ x_q^+ = \Delta_{p \to q}\left(x_p^-\right). \end{cases}$$

The model captures the continuous-time dynamics of the system in phase $p \in \mathcal{P}$ and the discrete transition to phase $q \in \mathcal{P}$, with the only valid choice of transitions for walking being $(p, q) \in \{(mc, sc), (sc, si), (si, sd), (sd, mc)\}$.

The switching surfaces, $\mathcal{S}_{p \to q}$, for the transitions for walking are defined by the zero level sets of the corresponding threshold functions $H_{p \to q} : TQ_s \to \mathbb{R}$, with, $H_{mc \to sc} := \theta_s - \theta_{mc}^-$, $H_{sc \to si} := q_{\mathrm{Bsp_{st}}} - 5^\circ$, $H_{si \to sd} := \theta_s - \theta_{si}^-$, and $H_{sd \to mc} := p_{\mathrm{toe_{sw}}}^v$. The transition maps, $\Delta_{p \to q} : S_{p \to q} \to TQ_s$, provide the initial conditions for the ensuing phase $q \in \mathcal{P}$, with, $\Delta_{mc \to sc} := \mathrm{id}$, $\Delta_{sc \to si} := \mathrm{id}$, $\Delta_{si \to sd} := \mathrm{id}$, and $\Delta_{sd \to mc} := \Delta_{s \to s}$, where id is the identity map and $\Delta_{s \to s}$ is as defined in Section II-C.

D. Fixed Point for Walking

A periodic walking gait is designed by selecting the free parameters in the virtual constraints. Using the hybrid system developed in the previous section, we formulate the problem as a constrained optimization to optimize the cost function J_1 specified in [13, Sec. 6.3.3]. This section presents a nominal fixed point of 0.8 m/s obtained by optimization. Figure 3 illustrates the nominal evolution of the virtual constraints and other configuration variables for one step. It is seen that the stance motor leg shape is held constant for the first part of the gait right after impact, and both the stance motor leg shape and the torso are held constant towards the final part of the gait. Interestingly, the torso moves less than two degrees throughout the step.

Figure 4 illustrates the evolution of the leg shape and the stance $\mathrm{B_{spring}}$ variables. Notice that the spring compresses to its peak value, and the $sc \to si$ transition is triggered as the spring decompresses to five degrees. The injection of energy in the si-phase causes the spring to compress again. Figure 5 illustrates the actuator torques used to realize the gait.

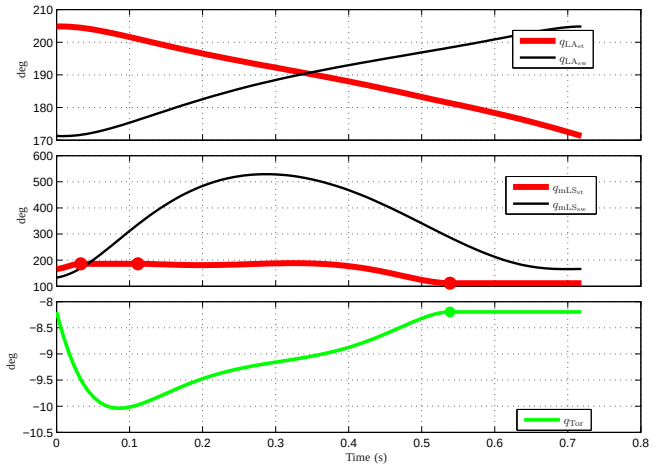

Fig. 3. Evolution of the virtual constraints and configuration variables for a nominal fixed point (periodic walking gait) at a speed of 0.8 m/s and step length 0.575 m. The dots on the stance motor leg-shape virtual constraint illustrate the location of transition between consecutive subphases.

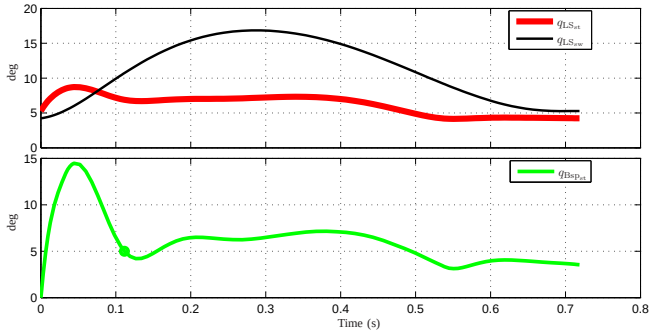

Fig. 4. Evolution of the leg shape and stance $\mathrm{B}_{\mathrm{spring}}$ variables corresponding to the nominal fixed point. The dot on the $\mathrm{B}_{\mathrm{spring}}$ plot illustrates the location of the *sc* to *si* event transition and corresponds to $q_{\mathrm{Bsp}_{\mathrm{st}}} = 5^{\circ}$.

These torques are small in comparison to the peak torque capacities of the actuators: 30 Nm at u_{mLA} and 55 Nm at u_{mLS}. The torques are discontinuous at phase boundaries, as noted earlier.

IV. Closed-loop Design and Stability Analysis

The feedback presented in (14) renders the zero dynamics manifold invariant under the stance phase dynamics. It is used in the optimization process of gait design in order to evaluate the torques along a solution of the model respecting the virtual constraints. The feedback (14) does not however render the solution stable or attractive in any way. The classic input-output linearizing controller

$$u = u^{*}\left(x_{\mathrm{s}}, \alpha_p\right) - L_{g_{\mathrm{s}}} L_{f_{\mathrm{s}}} h_p\left(q_{\mathrm{s}}, \alpha_p\right)^{-1} \left(\frac{K_{p,P}}{\epsilon^2} y + \frac{K_{p,D}}{\epsilon} \dot{y}\right), \tag{19}$$

with $p \in \mathcal{P}$ makes the zero dynamics manifold invariant and attractive [13, Chap 5].

This controller does not however, render the zero dynamics manifold hybrid invariant. It was discovered in [8], [7] that, in the presence of compliance, while the feedback controller

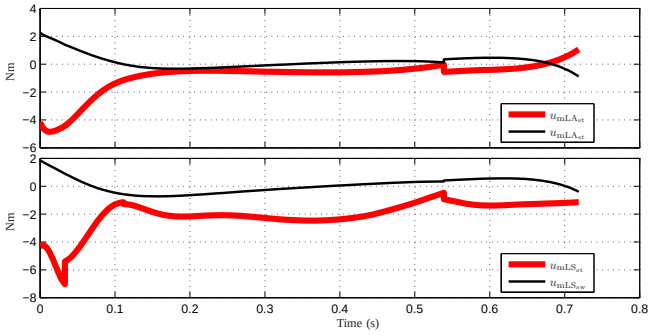

Fig. 5. Actuator torques corresponding to the nominal fixed point. Note that the torques are discontinuous at subphase boundaries, and as discussed in Section III-A.3, this occurs due to the choice of virtual constraints.

(19) will render the zero dynamics manifold of a given phase invariant under the continuous dynamics, it will not necessarily render it invariant under the transition maps, that is, at transitions from one phase to another, invariance is lost. The loss of invariance manifests itself as an impulsive disturbance to the control law at each transition off the periodic orbit. These perturbations do not prevent asymptotic stability from being achieved, but they do cause the actuators to do more work. The reference [7] proposed a supplemental event-based controller that eliminates this issue and, in fact, creates a *hybrid zero dynamics* for the closed-loop system, that is, the zero dynamics manifold is invariant under the continuous dynamics as well as the transition maps.

For the related robot, Thumper, [11] and [10] propose an event based control at each phase transition. This is not practical here, however, because we have certain phases with extremely small duration (the *mc* phase for instance). Here, we create a hybrid zero dynamics by updating parameters only at the impact event (swing leg contacts the ground).

Following [7], [15], the virtual constraints are modified stride to stride so that they are compatible with the initial state of the robot at the beginning of each step. The new output for the feedback control design is,

$$\begin{aligned} y_c &= h_{\mathrm{s}}\left(q_{\mathrm{s}}, y^{s+}, \dot{y}^{s+}\right) \\ &= H_0^{\mathrm{s}} q_{\mathrm{s}} - h_d^{\mathrm{s}}\left(\theta_{\mathrm{s}}\right) - h_c^{\mathrm{s}}\left(\theta_{\mathrm{s}}, y^{s+}, \dot{y}^{s+}\right). \end{aligned} \tag{20}$$

The output consists of the previous output, (7), and an additional correction term that depends on the previous output evaluated at the beginning of the step, specifically, $y^{s+} = H_0^{\mathrm{s}} q_{\mathrm{s}}^{+} - h_d^{\mathrm{s}}\left(\theta_{\mathrm{s}}^{+}\right)$, and $\dot{y}^{s+} = H_0^{\mathrm{s}} \dot{q}_{\mathrm{s}}^{+} - \frac{\partial h_d(\theta_{\mathrm{s}})}{\partial \theta_{\mathrm{s}}} \dot{\theta}_{\mathrm{s}}^{+}$. The values of y^{s+}, and $\dot{y}^{s+}$ are evaluated at the beginning of each step and held constant throughout the step. The function h_c^{s} is taken here as

$$h_c^{\mathrm{s}}\left(\theta_{\mathrm{s}}\right) = \begin{bmatrix} 0 \\ h_{\mathrm{LA}_{\mathrm{sw}}}^{c}\left(\theta_{\mathrm{s}}\right) \\ h_{\mathrm{mLS}_{\mathrm{sw}}}^{c}\left(\theta_{\mathrm{s}}\right) \\ h_{\mathrm{Tor}}^{c}\left(\theta_{\mathrm{s}}\right) \end{bmatrix}, \tag{21}$$

with each $h_v^c\left(\theta_{\mathrm{s}}\right)$, $v \in \mathcal{V}\backslash\{\mathrm{mLS}_{\mathrm{st}}\}$ taken to be twice

continuously differentiable functions of θ_{s} such that,

$$\begin{cases} h_v^c\left(\theta_{\mathrm{s}}, y^{s+}, \dot{y}^{s+}\right) & = y^{s+} \\ \frac{\partial h_v^c}{\partial \theta_{\mathrm{s}}}\left(\theta_{\mathrm{s}}^{+}\right) & = \frac{\dot{y}^{s+}}{\dot{\theta}_{\mathrm{s}}^{+}} \\ h_v^c\left(\theta_{\mathrm{s}}, y^{s+}, \dot{y}^{s+}\right) & = 0, \frac{\theta_{\mathrm{s}}^{+}+\theta_v^{mc+}}{2} \leq \theta_{\mathrm{s}} \leq \theta_v^{mc-} \end{cases}. \quad (22)$$

With h_v^c designed this way, the initial errors of the output and its derivative are smoothly joined to the original virtual constraint at the middle of the first phase of the corresponding virtual constraint. This is illustrated in Figure 2 with thick (red) dashed lines.

As noted in the definition of h_c^{s} in (21), we have enforced $h_{\mathrm{mLS_{st}}}^c \equiv 0$ since the *m*c phase is too short to handle significant transients without large actuator torques, and further we want to enforce the virtual constraint in the *s*c phase to be constant in order to effectively use the compliance. To overcome this, we propose an event-based control action specific for the $\mathrm{mLS_{st}}$ virtual constraint that updates $\alpha_{\mathrm{mLS_{st}}}^{mc}, \alpha_{\mathrm{mLS_{st}}}^{sc}, \alpha_{\mathrm{mLS_{st}}}^{si}$ at the beginning of each step such that during the *m*c phase, the virtual constraint only drives the motor leg shape velocity to zero, and during the *s*c phase, the virtual constraint keeps the motor shaft locked at a constant position. Not until the *s*i phase does the modified virtual constraint smoothly join the nominal virtual constraint. This correction term is also illustrated in Figure 2 with thick (red) dashed lines.

Under the new control law defined by (20), the behavior of the robot is completely defined by the event transition maps and the swing phase zero dynamics, with h_d^{s} replaced by $h_d^{\mathrm{s}}+h_c^{\mathrm{s}}$. The stability of the fixed-point x^* can now be tested numerically using a restricted Poincaré map $\rho : \mathcal{S} \cap \mathcal{Z} \rightarrow \mathcal{S} \cap \mathcal{Z}$ where $\mathcal{Z} = \{x_{\mathrm{s}} \in TQ_{\mathrm{s}} \mid y_c\left(q_{\mathrm{s}}\right) = 0, \dot{y}_c\left(q_{\mathrm{s}}\right) = 0\}$, the switching surface is taken to be the switching surface at the $si \rightarrow sd$ event transition, i.e., $\mathcal{S} = \mathcal{S}_{si \rightarrow sd}$, and

$$\rho\left(x_{\mathrm{s}}\right) = \phi\left(T_I \circ \Delta_{si \rightarrow sd}\left(x_{\mathrm{s}}\right), \Delta_{si \rightarrow sd}\left(x_{\mathrm{s}}\right)\right), \quad (23)$$

where, $\phi\left(t, x_0\right)$ denotes the maximal solution of (4), with initial condition x_0 at time $t_0 = 0$ and u as defined in (19). Hybrid invariance is achieved because the transition map for these events, $\Delta_{si \rightarrow sd}$ is the identity map, and $\Delta_{si \rightarrow sd}\left(\mathcal{S}_{si \rightarrow sd} \cap \mathcal{Z}\right) \subset \mathcal{S}_{si \rightarrow sd} \cap \mathcal{Z}$.

Using the restricted Poincaré return map (23), we can numerically calculate the eigenvalues of its linearization about the fixed-point. For the gait presented in the previous section, we obtain the eigenvalues

$$eig\left(\frac{\partial \rho\left(x_{\mathrm{s}}\right)}{\partial x_{\mathrm{s}}}\right) = \begin{bmatrix} 0.7258 \\ 2.6380e-5 \\ -1.8001e-6 \end{bmatrix}. \quad (24)$$

From [7, Cor. 2], the feedback (19) and (20) renders the periodic orbit of the closed-loop system exponentially stable for ϵ in (19) sufficiently small, and K_P, K_D such that $\lambda^2 + K_D\lambda + K_P = 0$ is Hurwitz.

V. Experimental validation of Compliant HZD Controller

This section documents experimental implementation of the compliant HZD controller of Section IV on MABEL focusing on achieving greater fidelity in the tracking of the virtual constraints. The controller was first coded in C++ and evaluated on a detailed simulation model of the robot that included encoder quantization and numerical estimation of velocity variables from encoder measurements. The controller was tested under various model perturbations, such as errors in the torso mass, spring stiffness, torso center of mass position, and deviations in initial conditions. These simulations are not discussed here for the sake of brevity. The simulation model was then replaced with the physical robot. The experimental protocol is identical to the one used in [6, Sect. 4]. Walking speed is measured with respect to the center point of the hip between the two legs. Video of the experiment is available on YouTube [16].

	$\mathbf{q}_{\mathrm{Tor}}$		$\mathbf{q}_{\mathrm{mLS_{st}}}$	
	PD	HZD	PD	HZD
RMSE	1.44°	0.89°	29.82°	0.28°
Peak	3.1°	2.4°	59.1°	39.5°

TABLE I

Error comparison between a PD and the compliant HZD based controller.

We report, for the first time, an experimental implementation of the full compliant hybrid zero dynamics controller to successfully achieve walking on MABEL. The virtual constraints depicted in Figure 3 are implemented with the full I/O linearizing controller (19), and with correction polynomials as in (20). The tracking accuracy obtained is far better than the PD controllers used previously [1]. The output coordinates are normalized to approximately the same magnitude for better conditioning of the decoupling matrix.

Figure 6 illustrates the tracking of q_{Tor} and $q_{\mathrm{mLS_{st}}}$, and Figure 7 illustrates the tracking of the swing leg virtual constraints. Table V compares the errors between a PD and the compliant HZD controller developed here.

Figure 8 illustrates the stance and swing $\mathrm{B_{spring}}$ values over a few steps. Notice that the $sc \rightarrow si$ transition occurs close to the designed value on one leg. Figure 9 depicts the control torques at the actuators, and are seen to be fairly noisy. The average walking speed for this experiment is 0.9 m/s. Figure 10 depicts the instantaneous power plot at the leg shape.

VI. Conclusion

A controller was designed to achieve exponentially stable walking while recruiting the compliance in the robot's drivetrain to perform most of the negative work required to decelerate the downward motion of the robot's center of mass after impact. This rendered the closed-loop system energy efficient and demonstrated the benefit of compliance even for walking. The analytically derived control law was experimentally validated on MABEL, resulting in the first ever real-time implementation of a complete hybrid zero dynamics based controller in experiments. The tracking accuracy attained was far better than that of simple PD controllers used in prior experiments on RABBIT, and MABEL.

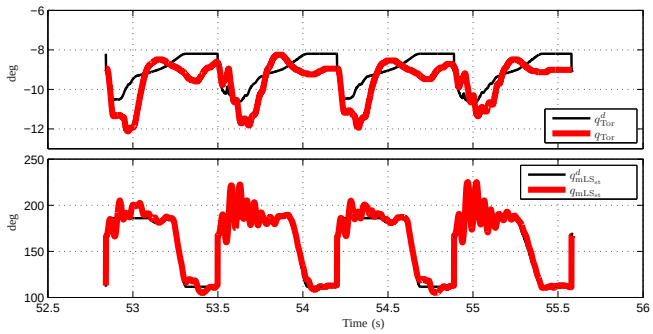

Fig. 6. Tracking for the stance virtual constraints for the compliant zero dynamics controller. This tracking fidelity is much improved with respect to PD controllers. However, there are significant oscillations in tracking the motor leg shape; these correspond to a peak variation of approximately 1.3° in q_{LS}.

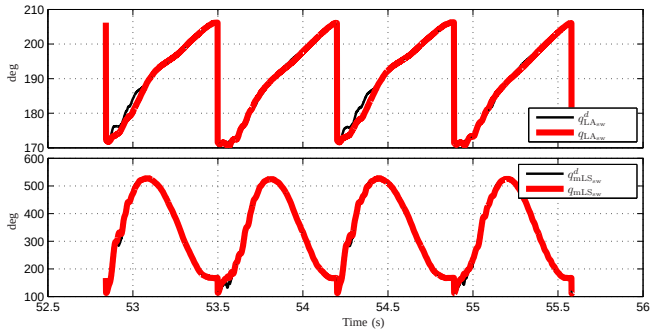

Fig. 7. Tracking of the swing leg virtual constraints for the compliant zero dynamics controller.

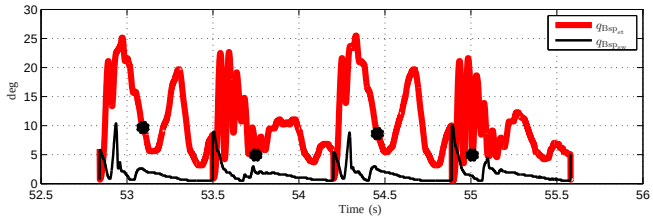

Fig. 8. $\mathrm{B}_{\mathrm{spring}}$ evolution for compliant zero dynamics controller. The asterisks indicate location of transition from the stance-compression (sc) to the stance-decompression (sd) phase.

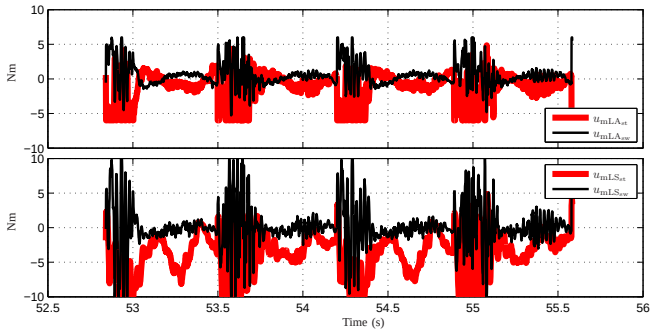

Fig. 9. Torques for the compliant zero dynamics controller. The torques appear 'noisy' and experience significant saturation (saturation limits were set to 6 Nm on leg angle motors and 10 Nm on leg-shape motors).

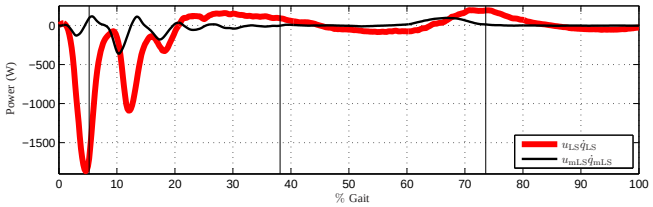

Fig. 10. Power plot averaged over 64 steps. The thick (red) line depicts the total instantaneous power at the leg shape from the actuator and the spring, and the thin (black) line depicts the instantaneous power at the leg shape from the motor alone. The difference is the energy that is saved and that would otherwise have to be provided by the actuator if the spring were absent. This plot shows the significant energy economy at impacts due to the presence of the compliance in the transmission.

REFERENCES

[1] K. Sreenath, H.-W. Park, I. Poulakakis, and J. W. Grizzle, "A compliant hybrid zero dynamics controller for stable, efficient and fast bipedal walking on MABEL," *International Journal of Robotics Research*, 2010, to appear, preprint available at [17].

[2] J. W. Grizzle, J. Hurst, B. Morris, H.-W. Park, and K. Sreenath, "MABEL, a new robotic bipedal walker and runner," in *American Control Conference*, Saint Louis, MO, USA, June 2009, pp. 2030–2036.

[3] J. W. Hurst, J. E. Chestnutt, and A. A. Rizzi, "Design and philosophy of the bimasc, a highly dynamic biped," in *IEEE International Conference on Robotics and Automation*, Roma, Italy, April 2007, pp. 1863–1868.

[4] H.-W. Park, K. Sreenath, J. W. Hurst, and J. W. Grizzle, "Identification and dynamic model of a bipedal robot with a cable-differential-based compliant drivetrain," University of Michigan Control Group, Tech. Rep. CGR 10-06, 2010, available at [17].

[5] R. Alexander, "Three uses for springs in legged locomotion," *The International Journal of Robotics Research*, vol. 9, no. 2, pp. 53–61, 1990.

[6] E. R. Westervelt, G. Buche, and J. W. Grizzle, "Experimental validation of a framework for the design of controllers that induce stable walking in planar bipeds," *The International Journal of Robotics Research*, vol. 23, no. 6, pp. 559–582, June 2004.

[7] B. J. Morris and J. W. Grizzle, "Hybrid invariant manifolds in systems with impulse effects with application to periodic locomotion in bipedal robots," *IEEE Transactions on Automatic Control*, vol. 54, no. 8, pp. 1751 – 1764, August 2009.

[8] B. Morris and J. W. Grizzle, "Hybrid invariance in bipedal robots with series compliance," in *IEEE Conference on Decision and Control*, San Diego, California, USA, December 2006.

[9] I. Poulakakis and J. W. Grizzle, "The spring loaded inverted pendulum as the hybrid zero dynamics of an asymmetric hopper," *IEEE Transactions on Automatic Control*, vol. 54, no. 8, pp. 1779–1793, August 2009.

[10] ——, "Modeling and control of the monopedal robot thumper," in *IEEE International Conference on Robotics and Automation*, Kobe, Japan, May 12-17 2009, pp. 3327–3334.

[11] I. Poulakakis, "Stabilizing monopedal robot running: Reduction-by-feedback and compliant hybrid zero dynamics," Ph.D. dissertation, The University of Michigan, 2008.

[12] A. Isidori, *Nonlinear Control Systems*, 3rd ed. Berlin: Springer-Verlag, 1995.

[13] E. R. Westervelt, J. W. Grizzle, C. Chevallereau, J. H. Choi, and B. Morris, *Feedback Control of Dynamic Bipedal Robot Locomotion*. Taylor & Francis/CRC Press, 2007.

[14] Y. Hürmüzlü and T. Chang, "Rigid body collisions of a special class of planar kinematic chains," *IEEE Transactions on Systems, Man and Cybernetics*, vol. 22, no. 5, pp. 964–71, 1992.

[15] J. W. Grizzle, C. Chevallereau, and C.-L. Shih, "HZD-based control of a five-link underactuated 3d bipedal robot," in *IEEE Conference on Decision and Control*, Cancun, Mexico, December 2008.

[16] J. W. Grizzle. (2010) Dynamic leg locomotion. Youtube Channel. [Online]. Available: http://www.youtube.com/DynamicLegLocomotion

[17] ——, "Jessy Grizzle's publications," 2009. [Online]. Available: http://www.eecs.umich.edu/~grizzle/papers